

Peptide Self-Assembled Nanostructures with Distinct Morphologies and Properties Fabricated by Molecular Design

Meiwen Cao,^{*,†,ID} Sha Lu,[†] Wenjing Zhao,[†] Li Deng,[†] Meng Wang,[†] Jiqian Wang,^{†,ID} Peng Zhou,[†] Dong Wang,[†] Hai Xu,^{*,†,ID} and Jian R. Lu^{*,†,ID}

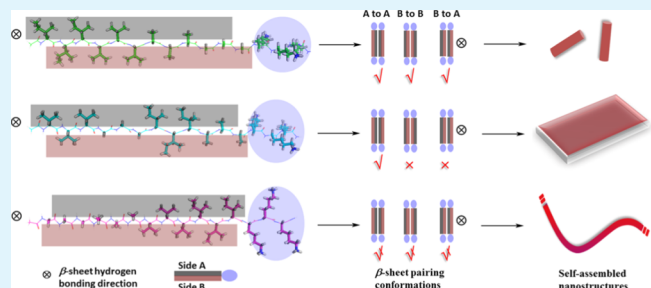
[†]State Key Laboratory of Heavy Oil Processing and Centre for Bioengineering and Biotechnology, China University of Petroleum (East China), 66 Changjiang West Road, Qingdao 266580, China

[‡]Biological Physics Laboratory, School of Physics and Astronomy, University of Manchester, Schuster Building, Oxford Road, Manchester M13 9PL, U.K.

Supporting Information

ABSTRACT: Six surfactant-like peptides with the same amino acid composition but different primary sequences are designed, including G₃A₃V₃I₃K₃, K₃I₃V₃A₃G₃, I₃V₃A₃G₃K₃, K₃G₃A₃V₃I₃, V₃G₃I₃A₃K₃, and K₃A₃I₃G₃V₃. These peptides form antiparallel β -sheets during self-assembly. Because the constituent residues have different side chain size and hydrophobicity, sequence changes adjust group distribution and hydrophobicity on the two sides of a given β -sheet. This consequently tunes the binding energy of the side-to-side pairing conformations and leads to different self-assembled structures. G₃A₃V₃I₃K₃ and K₃I₃V₃A₃G₃ form short nanorods with diameters of 8.5 ± 1.0 nm and lengths <150 nm. I₃V₃A₃G₃K₃ and K₃G₃A₃V₃I₃ form nanosheets with heights of 4.0 ± 0.5 nm and limited lengths and widths. V₃G₃I₃A₃K₃ and K₃A₃I₃G₃V₃ form long fibrils with diameters of 7.0 ± 1.0 nm and lengths of micrometer scale. These nanostructures exhibit different capacity in encapsulating insoluble hydrophobic drug molecules and delivering them into the cells. The nanosheets of I₃V₃A₃G₃K₃ and K₃G₃A₃V₃I₃ can encapsulate both nile red and doxorubicin molecules to an extent of up to 17–23% in mole ratio. Moreover, the shape and size of the nanostructures affect the drug delivery into cells greatly, with the nanosheets and short rods exhibiting higher efficiency than the long fibrils. The study provides new insights into programmed peptide self-assembly toward specific functionalities.

KEYWORDS: peptide self-assembly, primary sequence, nanostructures, β -sheet pairing, drug delivery, encapsulation



1. INTRODUCTION

The self-assembly of short peptides and even single amino acids has aroused great interests in recent years due to their great potential in producing a wide range of supramolecular nanostructures such as fibrils, vesicles, tubes, ribbons, tapes, honeycomb networks, and hydrogels.^{1–7} These nanostructures have found potential applications in materials science, biotechnology, and related fields by taking advantages of their distinct topographies.^{8–12} For example, fibrillar peptide nanostructures have been used as templates to fabricate one-dimensional inorganic materials;^{13,14} hydrogels comprised of fibrillar peptide nanostructures have been used as scaffolds for two- and three-dimensional cell culturing,^{15,16} and peptide nanostructures have also been used to assist the arrangement of porphyrins for fabrication of photoactive materials.^{17–19} Similar to lipid vesicles, vesicular peptide structures have been used as carriers for drug encapsulation and delivery.^{4,5,20–22} A common feature of the peptide nanostructures of different size and shape is the exhibition of tunable efficiency in cellular internalization and circulation.^{23–25} Therefore, fabrication of peptide nanostructures with well-defined structures from molecular design is

of great significance in the development of biocompatible drug-delivering biomaterials.

Peptide self-assembly is known to be a bottom-up process that is dictated by various noncovalent interactions such as electrostatic interaction, hydrogen bonding, hydrophobic interaction, and $\pi-\pi$ stacking.^{12,26,27} These interactions usually play different roles in driving peptide self-assembly along different dimensions and lead to anisotropic structural growth. Although most of the peptide nanostructures show a high aspect ratio, such as fibrils, ribbons, and tubes,^{8,9,11,28–31} two-dimensional lamellar structures^{21,22,32–34} have also been observed. The cross- β -sheet structure, where the long axial growth is perpendicular to the peptides backbone, is the basic element for templating these nanostructures.

Along the long axis, the nanostructure elongates upon stacking of peptide molecules into β -sheets via hydrogen bonding. The continuity of β -sheet hydrogen bonding growth

Received: August 6, 2017

Accepted: October 25, 2017

Published: October 25, 2017

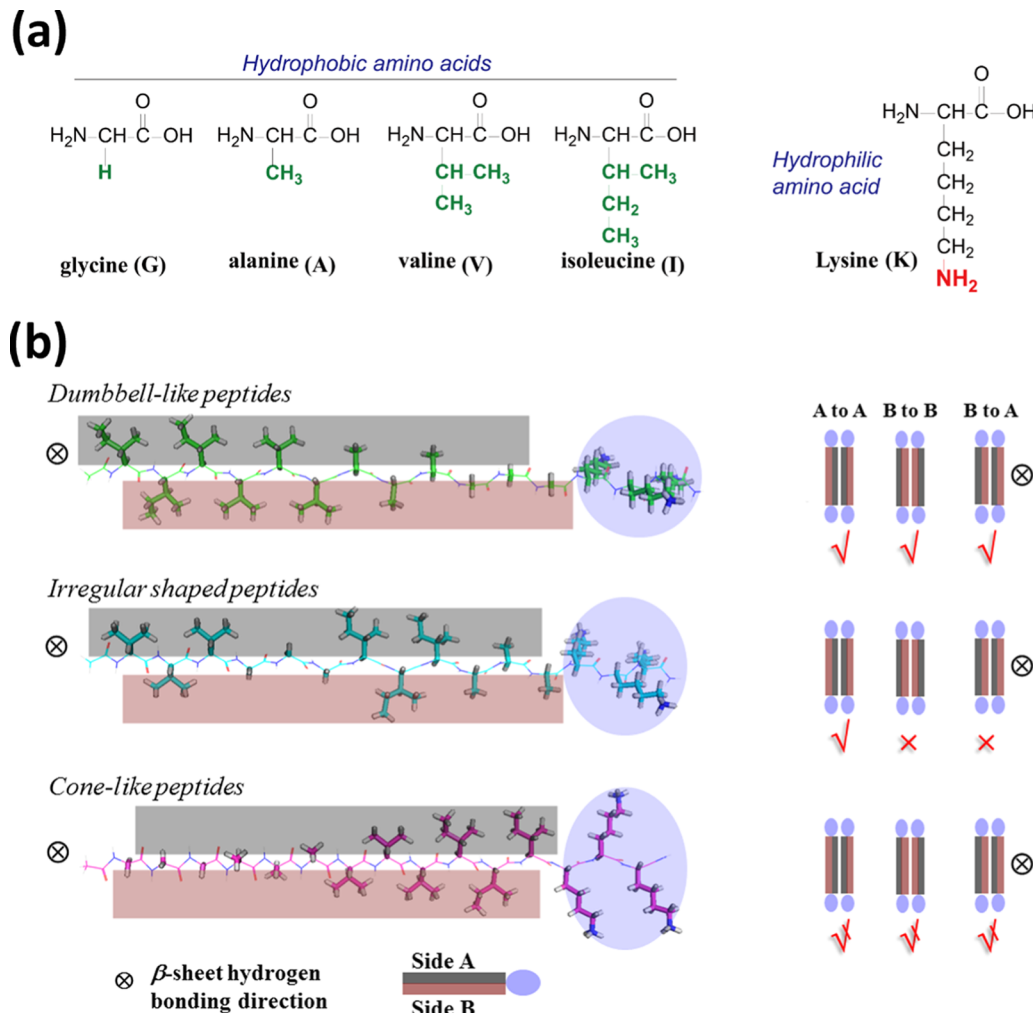


Figure 1. (a) Amino acids used in the design of the surfactant-like peptide molecules. (b) The molecular structures of the designed peptides. Distribution of the hydrophobic residues on the two faces of a β -strand is denoted by gray and magenta bars. The right panel shows the analysis of the possible interaction modes of the β -sheets.

along the long axis determines the length of the nanostructures. The distance between two peptides in the same cross- β -sheet is about 4.7 Å.^{35,36} Perpendicular to the long axis, the β -sheets are paired into “steric zippers” with hydrophobic complementary interfaces composed of side chains on each side of the β -sheets.^{22,37,38} The distance between two neighboring cross- β -sheets is about 10.0 Å.^{35,36} Usually, the distribution of side-chain groups on the two sides of a cross- β -sheet is not symmetrical. The lateral dimension along the zippering axis and/or diameter is determined by the stacking modes between side chains of the cross- β -sheets. Therefore, if one can control the β -sheet hydrogen bonding growth along the long axis and the β -sheet pairing along the zippering direction, programmed peptide self-assembly can be realized to produce nanostructures with well-defined morphologies.

Herein, we report on the fabrication of self-assembled peptide nanostructures with distinct morphologies by molecular design to control the higher-order arrangements of the β -sheets. Many simulation and experimental studies have found that surfactant-like peptides can easily self-assemble into β -sheets with antiparallel packing modes.^{34,39} To illustrate the effects from different packing modes of two peptide molecules when arranging into a β -sheet, we synthesized a series of surfactant-like peptides with the same amino acid composition

but varied molecular sequences (Figure 1). For each peptide, the polar region is made of three lysine (K) residues, whereas the nonpolar region is a 12-residue hydrophobic part consisting of glycine (G), alanine (A), valine (V), and isoleucine (I) residues. To exploit the benefit from the different size and hydrophobicity of the hydrophobic side chain residues, three repeats of each residue were used as a segment unit to construct the hydrophobic segment to amplify the sequence effect and adjust the distributions of side-chain groups on the two sides of a cross- β -sheet. Six peptides with different primary sequences were chosen and categorized by their molecular geometries, e.g., the cone-like peptides of G₃A₃V₃I₃K₃ and K₃I₃V₃A₃G₃, the dumbbell-like peptides of I₃V₃A₃G₃K₃ and K₃G₃A₃V₃I₃, and the irregular-shaped peptides of V₃G₃I₃A₃K₃ and K₃A₃I₃G₃V₃. Each pair of peptides in the same category has a reversed primary sequence and is different in terms of the positional disorder of the side-chain groups and the torsion angles.^{40,41} However, because they have the same side-chain group distribution on the two sides of a β -sheet, we expect similar self-assembled structures in them. Such a molecular design enables easy comparison between these peptides and assessment of the influence of these carefully selected sequences on the β -sheet arrangement and the subsequent self-assembly.

The six peptides have different ordering of the four hydrophobic segment units of GGG, AAA, VVV, and III. When stacking into antiparallel β -sheets, they will produce pairing interfaces with different surface group distributions (Figure 1). For the dumbbell-like peptides, e.g., I₃V₃A₃G₃K₃, the hydrophobic side-chain alkyl groups distribute relatively evenly on the two sides. “Side A” is summed to be about 16.4 on the hydrophobic scale,⁴² and “side B” is summed to be about 13.9. The close hydrophobicity of the two sides affords the pairing interactions of “A to A”, “B to B”, and “A to B” with similar binding energies and therefore enables extensive β -sheet packing along the zippering axis, which leads to nanostructures with extended lateral dimensions. For the irregular-shaped peptides, e.g., V₃G₃I₃A₃K₃, there is a dramatic difference in the distribution of the side-chain alkyl groups on the two sides of the β -sheets. The summed hydrophobicity of side A is 18.8, whereas that of side B is only 11.5. In this case, the A to A pairing interaction dominates the low binding energy and is the most stable one, whereas B to B and A to B pairing conformations are not favorable. The β -sheet packing along the zippering axis will then be limited by the weak stacking modes, and nanostructures with limited lateral dimensions are expected. The cone-like peptides were designed to have the same side-chain group distribution on the two sides of a β -sheet as that of the dumbbell-like peptides, but with different relative positions of the most hydrophobic segment of III and the charged segment of KKK. By linking the III segment directly to the KKK segment, we expect a weakened hydrophobic interaction due to the screening of hydrophobic interaction by steric effects. In this case, all of the three conformations of the β -sheet packing are expected to have lower stability. If the peptides do follow the proposed self-assembly routes as designed above, the final self-assembled nanostructures should be quite different for the three types of peptides.

2. EXPERIMENTAL SECTION

2.1. Materials. All of the peptides (purity >96%) were purchased from GL Biochem (Shanghai) Ltd. and used as received. Nile red (NR) was from Sinopharm Chemical Reagent Co., Ltd. All of the other chemicals including doxorubicin hydrochloride (DOX-HCl), thioflavin T (ThT), and 8-anilino-1-naphthalenesulfonate (ANS) were purchased from Sigma-Aldrich (China). Milli-Q water (18 M Ω cm) was used for all of the experiments.

2.2. Preparation of Peptide Solutions. Peptide solutions were prepared by directly dissolving the molecules in Milli-Q water. The pH of the solution was 4.2 \pm 0.3 due to residual trifluoroacetic acid in the peptide powder. All of the solutions were incubated at room temperature for at least 3 days before characterization so as to enable full equilibration of the solutions and avoid possible kinetic effects on the self-assembled structures.

2.3. Determination of the Critical Aggregation Concentration (CAC). The CAC of each peptide was determined by the fluorescence probe method, with pyrene as a probe molecule.⁴³ The peptide self-assembled structures can accommodate pyrene molecules by providing hydrophobic microenvironments and result in enhanced fluorescence intensity. The fluorescence intensity was measured on a microplate autoreader (Molecular Devices, M²e). For sample preparation, aliquots of 200 μ L peptide/pyrene mixed solution were added into each well of a 96-well plate. The concentration of pyrene was kept to be around 2 μ M whereas the peptide concentration was gradually increased. The solutions were excited at 335 nm, and the emission at 373 nm (I₁ band) was recorded. The CAC was determined by the intersection of the two linear fits in different concentration regions.⁴³

2.4. Atomic Force Microscopy (AFM). AFM measurements were performed in air using a Multimode Nanoscope VIII AFM system

(Bruker, Germany). Silicon probes of type TESPV-2 (320 kHz, 42 N/m) were used for image capturing. The sample was prepared by depositing 10 μ L of peptide solution onto a freshly cleaved mica surface. After adsorption for 30 s, the surface was dried with a nitrogen stream. Then, tapping mode images were recorded and analyzed with the NanoScope Analysis software (version 1.40, Bruker).

2.5. Transmission Electron Microscopy (TEM). A JEOL JEM-1400 equipment was used to carry out both negative-staining TEM and cryo-TEM measurements at an accelerating voltage of 200 kV. The negative-staining sample was prepared as follows. A carbon Formvar-coated copper grid was first placed on a drop of ~10 μ L peptide solution and adsorbed for 5 min. After wicking away the excess fluid by a filter paper, the grid was placed on a drop of uranyl acetate solution (2% w/v) for staining of ~2 min. The cryo-TEM samples were prepared with a controlled environment vitrification system. About 5 μ L of peptide solution was first deposited onto a copper grid with a laced support film. The excess solution was wicked away with filter papers and a thin solution film was formed on the mesh holes. The specimen was then quickly dipped into liquid ethane (-165 °C) for vitrification. The vitrified sample was then transferred to the cryogenic sample holder (Gatan 626) and examined at about -174 °C.

2.6. Circular Dichroism (CD). CD measurements were performed using a MOS-450/AF-CD spectrophotometer (BioLogic, France) at room temperature. A 0.2 mm quartz cell was used. Scans were collected in the range of 190–300 nm at 0.5 nm intervals. Averaging over three repeats were taken as the final results. Spectral smoothing was performed to reduce the noise with the help of the vendor-supplied software.

2.7. Attenuated Total Reflectance–Fourier Transform Infrared (ATR-FTIR) Spectroscopy. ATR-FTIR spectra were collected on a FTIR spectrometer (Nicolet 6700) equipped with a deuterated triglycine sulfate (DTGS) detector at room temperature. For spectra recording, an ARK HATR accessory containing a ZnSe crystal and a trough sampling plate was used. The peptides were dissolved in D₂O and incubated for 3 days for equilibrium. Then, the solutions were spread evenly on the ZnSe crystal plate for recording the spectra at a resolution of 4 cm⁻¹. For each sample, 256 scans were averaged to produce the final signal to reduce the noise.

2.8. Fluorescence Measurements. Fluorescence measurements were conducted using a Fluoro Max-P spectrophotometer (Jobin Yvon) at room temperature. A quartz cell of 0.5 cm path length was used. For ThT fluorescence measurements, the emission spectra in the range of 450–550 nm were recorded with excitation at 442 nm. For ANS fluorescence measurements, the emission spectra were collected in the range of 400–600 nm with excitation at 380 nm. For NR fluorescence measurements, the emission spectra in the range of 580–680 nm were obtained with excitation at 550 nm.

2.9. Small Angle Neutron Scattering (SANS). SANS spectra were collected on LOQ, ISIS Neutron Facility, Rutherford Appleton Laboratory (Oxford, U.K.). For sample preparation, the peptides were directly dissolved in D₂O. After aging for 3 days at room temperature, the samples were measured using disk-shaped silica cells with a path length of 2.0 mm. Neutron incident wavelength was set in the range of 2.2–10.0 Å at 25 Hz. The samples were placed at a distance of 4.05 m from the detector of 64 cm² and 5 mm resolution. The collected data were treated by first correcting for the incident spectrum, the wavelength dependence of the measured sample transmission, and relative detector efficiencies and then subtracting the D₂O background. A partially deuterated polystyrene standard was used for comparing the scattering to obtain the absolute scaling. All of the data were fitted using SansView 3.1.2. The models used for data fitting are detailed in Supporting Information.

2.10. X-ray Diffraction (XRD). XRD characterization was carried out on a panalytical X'pert Pro X-ray diffractometer with Cu K α radiation ($k = 1.54 \text{ \AA}$). The equipment was operated at 45 kV and 40 mA. The scan was performed at a rate 8°/min in the range of 5–75° (2 θ).

2.11. Drug Encapsulation and Release. Both NR and DOX were used as model drugs for drug encapsulation experiments. For measuring the NR-loading efficiency of different peptide nanostruc-

tures, the peptide solutions of 1.0 mM were first prepared and incubated for 3 days. Then, 200 μ L of peptide solutions were added into each well of a 96-well plate containing progressively increasing amount of NR. After shaking and incubating in dark for 2 h, the peptide/NR mixed solutions were taken for collecting the fluorescence emission at 630 nm on a fluorescence microplate reader (Molecular Instrument, M²e) with excitation at 550 nm. The fluorescence intensity was plotted as a function of the molar ratio of NR to peptide ($C_{NR}/C_{peptide}$). The saturation point of NR encapsulation was determined by the intercept of two linear fits extrapolating the data points from below and above the region in which a rapid change of slope is observed.⁴⁴

For DOX encapsulation, DOX-HCl was first treated with the following procedures to produce a hydrophobic DOX. Basically, 40 mg of DOX-HCl was added into a round-bottom flask (250 mL) with 80 mL of methanol/acetone (v/v = 1/1) mixture. Two hundred microliters of triethylamine was added dropwise into the solution and stirred at 37 °C for 24 h. Then, the solution was transferred to a dialysis tube (molecular weight cut-off = 3500) to remove the solvents. Finally, a freeze-dry procedure was performed to obtain the hydrophobic DOX, which was used for drug encapsulation into the peptide nanostructures with the same procedures as that of NR loading. For fluorescence measurements, the excitation was set at 480 nm and the emission collected at 580 nm. For evaluation of DOX release, 300 μ L of DOX-loaded peptide solution was dialyzed against 30 mL of Tris buffer solution. The release reservoir was kept under constant stirring, and 2 mL of the dialyzate was taken out at various time points for fluorescence measurement and 2 mL of fresh buffer solution was replenished to it.

2.12. Cytotoxicity Measurements and Cell Uptake of Peptide/DOX Composites. The peptides' cytotoxicity was evaluated by the tetrazolium reduction (3-(4,5-dimethylthiazol-2-yl)-2,5-diphenyltetrazolium bromide (MTT)) test. First, 100 μ L of HeLa cells in complete medium were added into each well of a 96-well plate at a density of 1×10^5 cells/mL. After culturing for 24 h at 37 °C for the cells to become adherent, the complete medium in each well was refreshed with 100 μ L of the new solution. Then, 100 μ L of peptide solution was added into each well. After culturing for another 24 h, 20 μ L of MTT solution (5 mg/mL) was added to each well and the plate was further incubated at 37 °C for 4 h. The supernatant was then aspirated thoroughly and 150 μ L of dimethyl sulfoxide (DMSO) was added to each well. Finally, the plate was shaken for 10 min to enable thorough mixing. A microplate reader was used to collect the absorbance at 570 nm. The cell survival ratio R was calculated by the following formula

$$R = 1 - (A_{Tris} - A_{peptide})/(A_{Tris} - A_{blank}) \quad (1)$$

where A_{Tris} is the absorbance of the medium, $A_{peptide}$ is the absorbance of the peptide/medium mixed solution, and A_{blank} is the absorbance of DMSO. Results were averaged from four parallel samples. The cells cultured in Tris buffer were used as control.

For testing the DOX delivery into cells by peptide nanostructures, the peptide/DOX composite solution was first dialyzed against 10 mL of Tris buffer. Then, 50 μ L of the composite solution was added into each well that had been preloaded with HeLa cells. After culturing at 37 °C for 24 h, the cells were imaged on a microscope (Leica DMI3000B) equipped with an oil-immersion objective ($\times 100$).

3. RESULTS AND DISCUSSION

3.1. Peptide Self-Assembly and Characterization.

Being identical in chemical composition, the six peptides of G₃A₃V₃I₃K₃, K₃I₃V₃A₃G₃, I₃V₃A₃G₃K₃, K₃G₃A₃V₃I₃, V₃G₃I₃A₃K₃, and K₃A₃I₃G₃V₃ have similar overall hydrophobicity and pK_a, with CACs within a relatively narrow range of 0.2–1.0 mM (Figure 2). K₃G₃A₃V₃I₃ and V₃G₃I₃A₃K₃ have CACs of 0.28 and 0.97 mM, respectively, but the other four peptides gave similar CACs of ~0.6 mM. An interesting observation was that the fluorescence intensities of the two

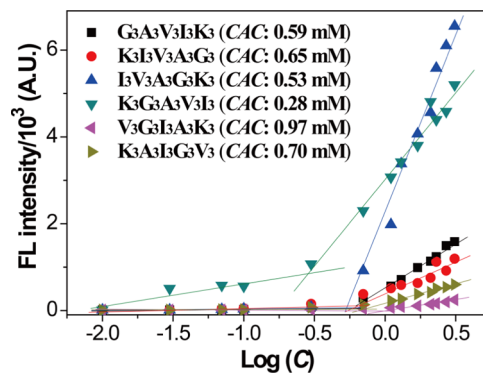


Figure 2. CACs as determined by the pyrene fluorescence through the intersection of the two linear fits in different concentration regions. All of the peptide solutions are at pH 4.0 \pm 0.2.

dumbbell-like peptides are much larger than those of the other four peptides at concentrations above the CACs. Because the fluorescence intensity is indicative of the quantity and/or hydrophobicity of the aggregates, the results indicate that the aggregates of the dumbbell-like peptides either are larger in quantity or provide microenvironments with much higher hydrophobicity.⁴³

Cryo-TEM revealed that the three categories of peptides self-assembled into different nanostructures at concentrations above their CACs, and similar results were also observed from negative-staining TEM and AFM (Figure 3). The morphologies of these nanostructures show a clear dependence on the primary sequence. The cone-like peptides of G₃A₃V₃I₃K₃ and K₃I₃V₃A₃G₃ self-assemble into short nanorods with diameters of 8.5 ± 1.0 nm and lengths of less than 150 nm (Table 1). The irregular-shaped peptides of V₃G₃I₃A₃K₃ and K₃A₃I₃G₃V₃ form long nanofibrils with diameters of 7.0 ± 1.0 nm and lengths of micrometer scale. The dumbbell-like peptides of I₃V₃A₃G₃K₃ and K₃G₃A₃V₃I₃ both form flat nanosheets of different sizes. The I₃V₃A₃G₃K₃ nanosheets have lengths of less than 100 nm and widths of 20 ± 10 nm. The K₃G₃A₃V₃I₃ nanosheets are slightly longer and wider, with lengths of less than 150 nm and widths of 30 ± 20 nm. AFM sectional profiles give similar heights of 4.0 ± 0.5 nm (Figure 3c,d, insets). Due to the low contrast between these thin assemblies and the ice substrate layer, their cryo-TEM images are somewhat blurred, but the nanosheets with larger lateral sizes can still be distinguished. These self-assembled nanostructures could also be found at lower concentrations slightly above the CACs (Figure S1). Experiments with different batches of peptides also produced the same nanostructures. Therefore, the self-assembled nanostructures are reproducible. The effect of pH on their self-assembly has also been investigated. At higher pH of 10.0 \pm 0.5, the self-assembled structures exhibited an increased propensity for lateral association in all of the cases and the short fibrils of the cone-like peptides showed larger lengths (Figure S2). These changes must arise from deprotonation of the Lys residues, which reduces charge repulsion among aggregates and facilitates molecular arrangement along the long axis.

The structural characteristics of these peptide nanoassemblies were further explored at shorter length scale by SANS measurements (Figure 4 and Table S1 in the Supporting Information).^{45,46} It can be seen from Figure 4 that in all of the cases, the SANS intensity (I) versus the wave vector transfer (q) shows an approximate dependence of $I \propto q^{-2}$ at $q < 0.1$, i.e.,

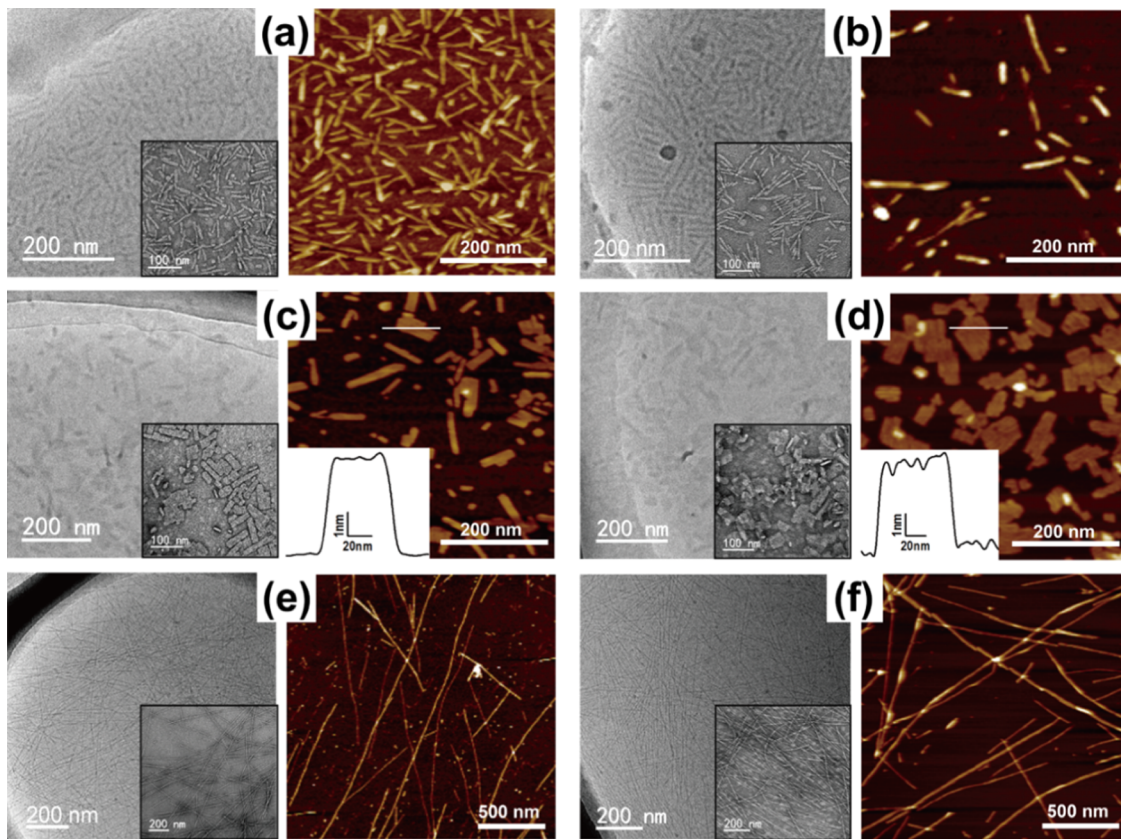


Figure 3. Cryo-TEM (left panel), negative-staining TEM (insets of left panel), and AFM (right panel) images showing the self-assembled structures of (a) $\text{G}_3\text{A}_3\text{V}_3\text{I}_3\text{K}_3$, (b) $\text{K}_3\text{I}_3\text{V}_3\text{A}_3\text{G}_3$, (c) $\text{I}_3\text{V}_3\text{A}_3\text{G}_3\text{K}_3$, (d) $\text{K}_3\text{G}_3\text{A}_3\text{V}_3\text{I}_3$, (e) $\text{V}_3\text{G}_3\text{I}_3\text{A}_3\text{K}_3$, and (f) $\text{K}_3\text{A}_3\text{I}_3\text{G}_3\text{V}_3$ at 4.0 mM and pH of 4.0 ± 0.2 .

Table 1. Main Size Parameters Measured from the Self-Assembled Peptide Nanostructures

peptides	self-assembled structures	sizes (diameter (d) ^a , length (l) ^{a,b} , width (w) ^{a,c} , thickness (h) ^c)
$\text{G}_3\text{A}_3\text{V}_3\text{I}_3\text{K}_3$	short fibers	$d: 8.5 \pm 1.0 \text{ nm}$, $l: < 100 \text{ nm}$
$\text{K}_3\text{I}_3\text{V}_3\text{A}_3\text{G}_3$	short fibers	$d: 8.5 \pm 1.5 \text{ nm}$, $l: < 150 \text{ nm}$
$\text{I}_3\text{V}_3\text{A}_3\text{G}_3\text{K}_3$	flat sheets/tapes	$h: 4.0 \pm 0.5 \text{ nm}$, $l: < 200 \text{ nm}$, $w: 20 \pm 10 \text{ nm}$
$\text{K}_3\text{G}_3\text{A}_3\text{V}_3\text{I}_3$	flat sheets/tapes	$h: 3.9 \pm 0.5 \text{ nm}$, $l: < 150 \text{ nm}$, $w: 30 \pm 20 \text{ nm}$
$\text{V}_3\text{G}_3\text{I}_3\text{A}_3\text{K}_3$	long fibrils	$d: 7.2 \pm 1.0 \text{ nm}$, $l: \text{micrometers}$
$\text{K}_3\text{A}_3\text{I}_3\text{G}_3\text{V}_3$	long fibrils	$d: 6.8 \pm 0.8 \text{ nm}$, $l: \text{micrometers}$

^aDetermined from the cryo-TEM results. ^bDetermined from the negative-staining TEM results. ^cDetermined from the AFM results.

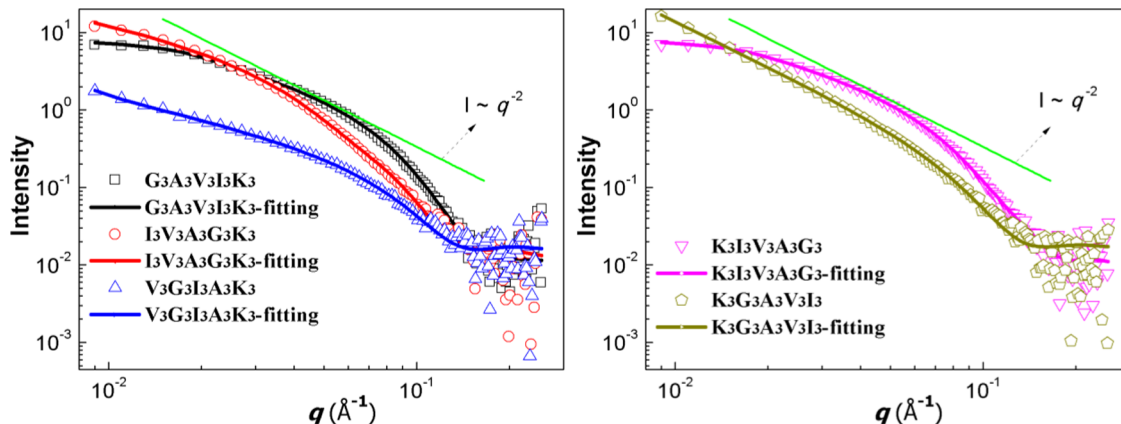


Figure 4. SANS profiles from different peptide solutions at 16.0 mM and pH 4.0 ± 0.2 . The profile of $\text{K}_3\text{A}_3\text{I}_3\text{G}_3\text{V}_3$ is absent due to solubility problem during sample preparation at this solution condition. The $I \sim q^{-2}$ feature is plotted for comparison.

with the slope of -2 in the log I -log q plot. Such results indicate that all of the peptide nanostructures are comprised of

lamellar units.^{31,47} Further analysis of these data helped to reveal more detailed structural characteristics. For the cone-like

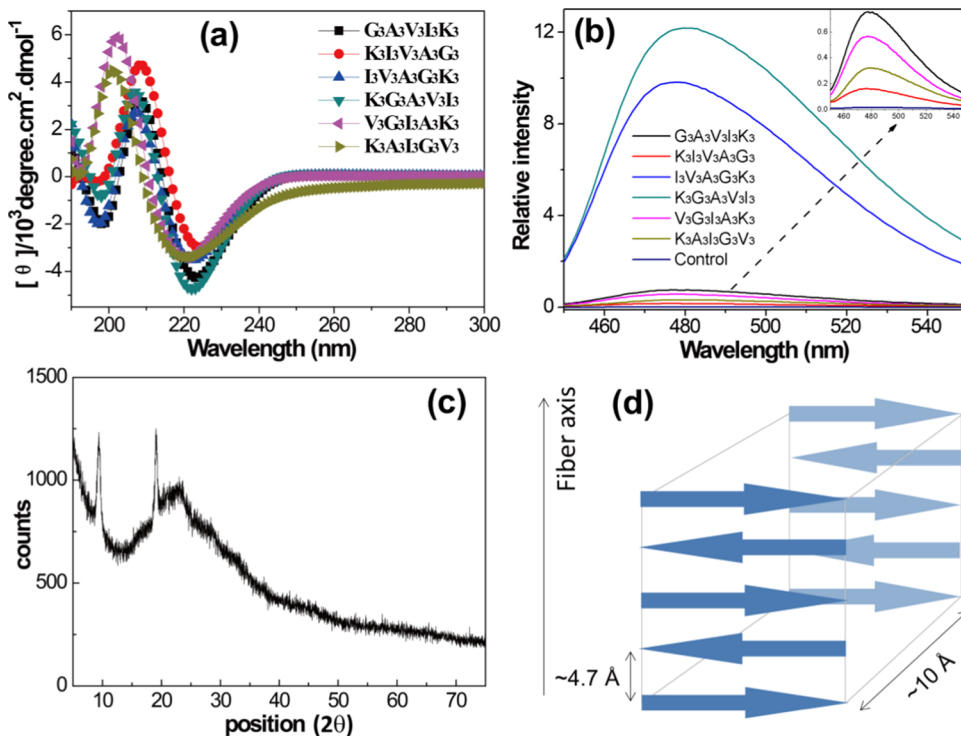


Figure 5. (a) CD spectra of the peptides at 4.0 mM and pH 4.0 ± 0.2 . (b) ThT fluorescence emission spectra of the peptide/ThT mixed solutions. The solution of ThT in pure water was used as control. (c) Representative XRD spectrum obtained from freeze-drying powders of $I_3V_3A_3G_3K_3$ (obtained from solution of 4.0 mM and pH 4.0 ± 0.2). (d) Scheme showing the characteristic cross- β -spacings from XRD.

peptides of $G_3A_3V_3I_3K_3$ and $K_3I_3V_3A_3G_3$, a flexible cylinder ellipsoidal model was found to fit the data well, giving ellipsoidal cylinders with limited lengths and the major diameters of ~ 6.7 and ~ 7.7 nm, respectively. These results correlate well with the nanorods observed by TEM and AFM. For the irregular-shaped peptides of $V_3G_3I_3A_3K_3$ and $K_3A_3I_3G_3V_3$, a cylinder model fitted the data well with lengths of >100 nm (beyond the limit of SANS fitting) and a diameter of ~ 4.9 nm, again consistent with the long fibrillar structures. However, for the dumbbell-like peptides of $I_3V_3A_3G_3K_3$ and $K_3G_3A_3V_3I_3$, no single model could fit the SANS data well, whereas a lamellar model and an elliptical cylinder model together provided the best fit. For $I_3V_3A_3G_3K_3$, the predicted structures were tapes of length ~ 26 nm, height ~ 4.7 nm, and width ~ 14 nm (elliptical cylinder model), and lamellae with a thickness of ~ 4.8 nm (lamellar model). For $K_3G_3A_3V_3I_3$, the predicted structures were elliptical cylinders of length ~ 20 nm, height ~ 4.0 nm, and width ~ 6.4 nm, and lamellae with a thickness of ~ 4.1 nm. The limited length values in the two cases correspond well with the TEM and AFM results, with a limited length of <150 nm. The fitted thickness values were slightly larger than the ones obtained from the AFM profiling, which were ~ 4.3 and ~ 3.9 nm for $I_3V_3A_3G_3K_3$ and $K_3G_3A_3V_3I_3$, respectively. The differences could arise from the pressure exerted by the AFM tip against the soft nanostructures.

The secondary structures of the peptides were then assessed using CD and FTIR. From the CD spectra obtained at 0.5 mM (Figure S5), all of the peptides except $K_3G_3A_3V_3I_3$ gave a negative maximum at around 201 nm, indicating that these peptides adopted mainly random coiled conformations. $K_3G_3A_3V_3I_3$, on the other hand, gave a positive maximum at 205 nm and a negative maximum at 221 nm, characteristic of β -sheet secondary structures. The result was consistent with

$K_3G_3A_3V_3I_3$ having the lowest CAC of 0.28 mM in this series (Figure 2). At 4.0 mM, a concentration above their CACs, all of the peptides show typical β -sheet CD signals (Figure 5a). Specifically, the cone-like peptides ($G_3A_3V_3I_3K_3$ and $K_3I_3V_3A_3G_3$) and the dumbbell-like peptides ($I_3V_3A_3G_3K_3$ and $K_3G_3A_3V_3I_3$) all exhibit a positive maximum around 207 nm and a negative maximum around 222 nm, whereas the irregular-shaped peptides ($V_3G_3I_3A_3K_3$ and $K_3A_3I_3G_3V_3$) have a positive maximum at ~ 201 nm and a negative maximum at ~ 220 nm. It has been demonstrated that classical β -sheet structures present a maximum at 195 nm and a minimum at 218 nm.⁴⁸ The peak shifts for the peptides studied here indicate a possible distortion of the β -sheets or varied packing modes.⁴⁹ For the irregular-shaped peptides, the CD peaks gave the smallest red-shifts, indicating that the β -sheets in the long fibrils are little changed from their intrinsic twisting. For the cone-like peptides and the dumbbell-like peptides, the CD peaks show relatively larger red-shifts, probably indicating that the β -sheets adopt more distorted conformations to satisfy the requirements of specific shape and curvature of the self-assembled structures of either the short rods or the lamellar nanosheets.

The β -sheet secondary structures were further confirmed by FTIR measurements (Figure S6), with characteristic absorbance peaks at 1629, 1661, and 1676 cm^{-1} , respectively. The peak at 1629 cm^{-1} can be assigned to the β -sheet conformation, whereas the peak at 1676 cm^{-1} indicates that these β -sheets are antiparallel.^{50,51} Taken together, despite the different self-assembled structures, β -sheets are the common building units. The results agree well with the SANS data, also unraveling the basic lamellar self-assembling units.

The structural characteristics of the peptide nanostructures were further assessed by the ThT binding assay, with the results shown in Figure 5b. Against the control, the ThT fluorescence

Table 2. Structural Periodicities Derived from the XRD Spectra As Shown in Figures 5c and S7

peptides	G ₃ A ₃ V ₃ I ₃ K ₃	K ₃ I ₃ V ₃ A ₃ G ₃	I ₃ V ₃ A ₃ G ₃ K ₃	K ₃ G ₃ A ₃ V ₃ I ₃	V ₃ G ₃ I ₃ A ₃ K ₃	G ₃ A ₃ V ₃ I ₃ K ₃
intersheet distance (Å)	10.45		9.42	9.70	10.30	10.25
interstrand distance (Å)	4.65	4.68	4.64	4.66	4.65	4.62

emission around 480 nm shows a significant increase for all of the peptides, indicating that the short rods, the lamellae nanosheets, and the long fibrils are all amyloid-like in nature. These nanostructures all have the cross- β -structure with the β -strands aligned perpendicular to both the long axis of the assembly and the lamination of the β -sheets.^{52–54} Interestingly, the two dumbbell-like peptides of I₃V₃A₃G₃K₃ and K₃G₃A₃V₃I₃ show much larger fluorescence intensities than the other four peptides. It has been reported that ThT molecules are bound either by intercalating between two adjacent peptide chains or directly on top of the peptide strands.^{55,56} Therefore, the difference in fluorescence intensity indicates that the mode of β -sheet arrangement in the nanosheets is different from that in the nanorods and long fibrils.^{55–57}

XRD was further used to probe the internal β -sheet arrangements in these assemblies. Figure 5c shows the typical XRD spectrum for I₃V₃A₃G₃K₃. The spectrum shows two sharp reflections at 8.9 ± 0.6 and $19.1 \pm 0.2^\circ$, corresponding to *d*-spacings of around 10.5 and 4.7 Å, respectively. The 10.5 Å periodicity is ascribed to the intersheet distance between laterally stacked β -sheets.^{35,36} The 4.7 Å signal is a typical distance that can be ascribed to the separation between hydrogen-bonded β -strands.^{35,36} These periodicities correlate well with a cross- β -diffraction pattern. The spectra for other five peptides (Figure S7) show similar results to that of I₃V₃A₃G₃K₃ and the derived size parameters for all of the peptides are listed in Table 2. A common cross- β -structure can be deduced from the XRD results, as shown in Figure 5d. Noting that the intersheet distances of the two dumbbell-like peptides are smaller than those of the other four peptides at a value of more than 0.6 Å, we deduce that the β -sheets pack more tightly in the lamellar belt structures than in the nanorods/fibrils. Such a variation in *d*-spacing value is suggested to relate closely to the side-chain interactions.

Thus, the self-assembly results correlate well with those expected from our molecular design. Although the six peptides have the same amino acid composition, they can be well manipulated to form three distinct kinds of nanostructures by molecular design. The dumbbell-like peptides form lamellar nanosheets, the irregular-shaped peptides form long fibrils, and the cone-like peptides form short nanorods, although all of these nanostructures have β -sheets as the fundamental building unit. It is therefore the higher-order arrangement of the β -sheets that determines the final morphologies of the self-assembled nanostructures, as proposed in Figure 1. For the dumbbell-like peptides, the three β -sheet pairing conformations have similar binding energies and extensive β -sheet packing along the zippering axis to form lamellar structures. For the irregular-shaped peptides, only one pairing conformation dominates with a low binding energy and prevails over the other two. This disables the β -sheet packing along the zippering axis and results in the blocking of lamella formation. It is further demonstrated that the two reverse-sequenced peptides in one category produce nanostructures with similar morphology.

The particular feature of the cone-like peptides in forming short nanorods is explained as follows. Because the most hydrophobic segment of III is connected directly to the charged

segment of KKK, the hydrophobic interaction of the nearest one or two isoleucine residues is greatly affected by steric effects and electrostatic repulsion. In this case, the overall hydrophobic interaction is weakened and the difference between the three pairing conformations is increased. This limits the ability of β -sheet stacking along the zippering axis to extend the lateral size.

However, there are several other interesting observations waiting to be explained. First, although the two molecules with reversed sequence in one category form nanostructures with similar morphology, their sizes do show some differences. This is especially so for the two dumbbell-like peptides. The nanosheets of K₃G₃A₃V₃I₃ are slightly larger than those of I₃V₃A₃G₃K₃, with the widths being 30 ± 20 and 20 ± 10 nm, respectively. K₃G₃A₃V₃I₃ has its charged lysine residues on the acetylated N-terminal, whereas I₃V₃A₃G₃K₃ has them on the amidated C-terminal. Therefore, the electrostatic repulsion among K₃G₃A₃V₃I₃ molecules should be lower than that of I₃V₃A₃G₃K₃, which is supposed to be more favorable for growth of the nanosheets into larger ones by facilitating β -sheet stacking.³¹ Second, though the six peptides have the same extended chain length, the diameters are quite different for the nanorods of the cone-like peptides (8.5 ± 1.0 nm) and the fibrils of the irregular-shaped peptides (7.0 ± 1.0 nm). This is mainly due to the different number of β -sheets involved in the zippering axial packing and twisting. Moreover, the lengths of the nanorods of the cone-like peptides and the nanosheets of the dumbbell-like peptides are limited to be <150 nm. Such a self-limitation in the axial growth is suggested to be due to noncontinuity of the β -sheet hydrogen bonding due to conformational constraint during nanostructure growth.

3.2. Drug Encapsulation and Delivery. By having the same amino acid composition but distinct self-assembled nanostructures, the six peptides here offer a good opportunity to probe into the effects of shape and size of the self-assembled structures on drug loading and delivery.²⁵ The peptide nanostructures can provide hydrophobic inner cores for the incorporation of hydrophobic and sparingly soluble drug molecules.^{44,58} First, the polarity inside each nanostructure was evaluated by using 8-anilino-1-naphthalenesulfonate (ANS) as a fluorescent probe (Figure S8 and Table 3).^{44,59} The polarity inside the nanosheets of I₃V₃A₃G₃K₃ and K₃G₃A₃V₃I₃ corresponded to an E_T^N value of 0.72 and 0.74, respectively, between that of methanol ($E_T^N = 0.76$) and ethanol ($E_T^N = 0.65$).⁵⁹ The short rods of the cone-like peptides and the long fibrils of the irregular-shaped peptides all gave relatively higher E_T^N values between 0.85 and 0.80, slightly higher than that of methanol. The drug encapsulation tests were performed with two hydrophobic model drugs, a dye of nile red (NR) and an anticancer drug of DOX. In water, NR gave a quite low fluorescence emission, with peak at 654 nm (Figure 6a), consistent with few dissolved NR molecules in a hydrophilic environment.⁴⁴ After being dissolved in peptide solutions, the NR fluorescence intensity was significantly enhanced, indicating a much higher amount of NR dissolution. Moreover, the peaks all shift toward lower wavelength to be below 640 nm, indicating the incorporation of NR into the hydrophobic inner

Table 3. Internal Polarity and the Relative NR/DOX Loading Efficiency of Each Peptide Nanostructure

peptide	$(E_T^N)^a$	LC _{NR} (%) ^b	LC _{DOX} (%) ^b
control (water)	1.0		
G ₃ A ₃ V ₃ I ₃ K ₃	0.81	5.4	10.7
K ₃ I ₃ V ₃ A ₃ G ₃	0.82	4.5	11.8
V ₃ G ₃ I ₃ A ₃ K ₃	0.84	6.1	8.4
K ₃ A ₃ I ₃ G ₃ V ₃	0.83	6.4	12.5
I ₃ V ₃ A ₃ G ₃ K ₃	0.72	17.1	19.7
K ₃ G ₃ A ₃ V ₃ I ₃	0.74	22.6	20.4

^a E_T^N is a normalized polarity scale that can be determined by the peak wavelength of ANS.⁵⁹ E_T^N works well in detecting the internal polarity of peptide nanostructures.⁴⁴ ^bLC_{NR} (LC_{DOX}) is the relative NR (DOX) loading capacity of peptide nanostructures, presented as the mole ratio of NR (DOX) to peptide.

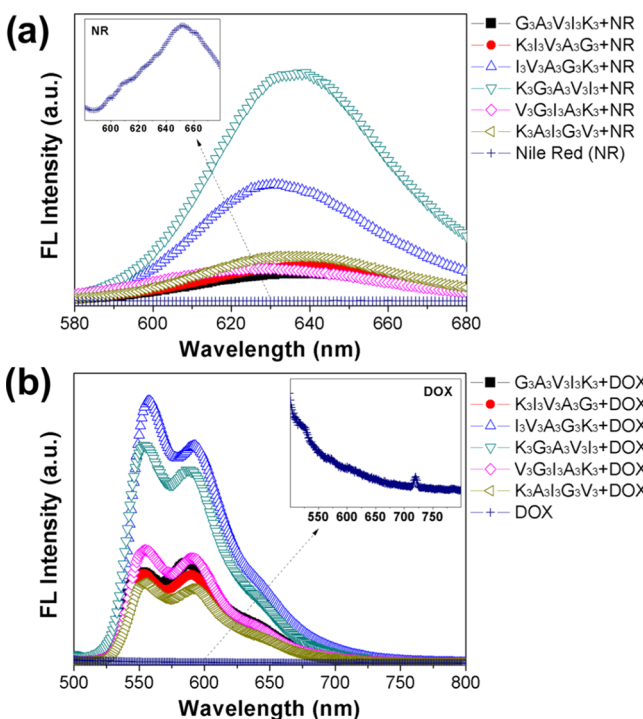


Figure 6. Fluorescence spectra of (a) NR and (b) DOX in different peptide solutions of 4.0 mM and pH 4.0 ± 0.2. The samples of NR/DOX in water were used as control.

cores.^{44,58} Similarly, DOX could hardly be dissolved in water as verified by the absence of fluorescence emission peaks in the aqueous solution (Figure 6b). However, when dissolved in peptide solutions, the fluorescence spectra of DOX showed a significant increase in the intensity and gave two peaks at around 553 and 590 nm, also indicating the enhanced solubility of DOX by incorporating into the hydrophobic environments of the peptide nanostructures. The drug-loading efficiency of each peptide was further determined (Table 3, Figures S9 and S10). The peptides of G₃A₃V₃I₃K₃, K₃I₃V₃A₃G₃, V₃G₃I₃A₃K₃, and K₃A₃I₃G₃V₃ gave loading efficiencies of 5–7% for NR and 8–13% for DOX. The peptides of I₃V₃A₃G₃K₃ and K₃G₃A₃V₃I₃ gave a relatively higher loading efficiencies, 17–23% for NR, and 19–21% for DOX, respectively. With respect to the nanostructures, the nanosheets exhibited a higher drug-loading efficiency than the short nanorods and the long fibrils.

The drug release was also evaluated for the DOX-loaded peptide nanostructures. The results (Figure S11) show that in

all of the cases the variation in DOX concentration in the dialyzate followed a sigmoidal profile with time. Noting that intermittent replenishment of the dialyzate was performed, the results indicate a gradual increase in the total released DOX.

Experiments were further made to test the possibility of using these nanostructures for drug delivery. The cytotoxicity of each peptide was first assessed with the MTT assay. The results (Figure S12) show that all of the peptides gave the survival ratio of >70% at the peptide concentration of 4.0 mM over the assessment period, indicating a relatively low toxicity. Then, the intracellular delivery experiments were carried out by coculturing the DOX-loaded peptide nanostructures with HeLa cells. The results show that for the peptides of K₃G₃A₃V₃I₃ (Figure 7a) and K₃I₃V₃A₃G₃ (Figure 7b), the

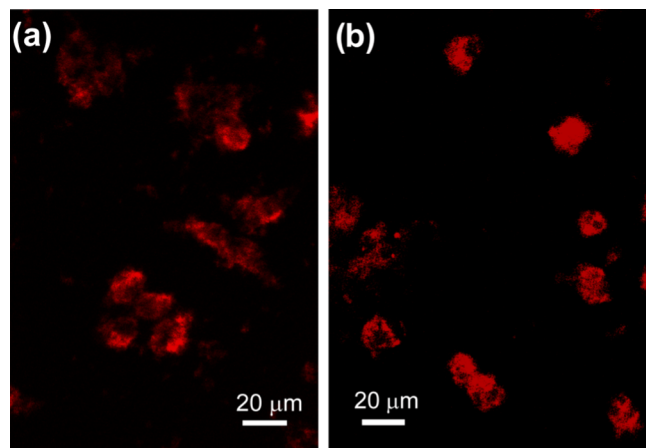


Figure 7. Inverted fluorescence microscopy images of the HeLa cells treated with the DOX-loaded peptide nanostructures: (a) K₃G₃A₃V₃I₃ and (b) K₃I₃V₃A₃G₃.

cells were brightly fluorescent after the coculturing process, whereas for K₃A₃I₃G₃V₃, no obvious fluorescence could be observed (data not shown). The results indicate that the nanosheets and the short nanorods were more efficient than the long fibrils in delivering drug molecules into the cells. This highlights the importance of shape and size of the nanostructures on their drug delivery efficiency. For the nanosheets and the short nanorods, their smaller sizes and the multivalent nature were the likely reasons for their higher efficiency.²³ However, for the long fibrils, their large length might prevent them from cell internalization. Moreover, most of the DOX molecules were distributed in the cytoplasm, indicating the possible site of the cargo-unloading.

4. CONCLUSIONS

The present study shows that even peptides with the same amino acid composition could be designed via sequence variation to have the right codes for self-assembling into nanostructures with distinct morphologies. Sequence changes in selected order of groups affected the side-chain distribution on the two sides of a β-sheet, which consequently determines the β-sheet packing along the zipper axis. The dumbbell-like peptides formed β-sheets with close hydrophobicity for the two sides, with the three β-sheet pairing conformations of A to A, B to B, and A to B showing similar binding energy. This enabled the extensive β-sheet packing along the zipper axis to form nanosheets. In contrast, the irregular-shaped peptides formed β-sheets with the two sides having dramatic difference in

hydrophobicity. In this case, only one face-to-face pairing conformation became the most stable one. The β -sheet packing along the zipper axis was restricted, resulting in the formation of fibrils. On the other hand, the cone-like peptides formed β -sheets with similar hydrophobicity distribution on the two sides to those of the dumbbell-like peptides. However, the cone-like peptides have the most hydrophobic isoleucine residues directly connected to the charged lysine residues. The hydrophobic interaction involving isoleucines is greatly restricted due to the steric effect. This restrained both the β -sheet hydrogen bonding extension and the β -sheet stacking along the zipper axis, resulting in the formation of short nanorods. Therefore, this study provides new insights into the modulation of peptide self-assembled nanostructures by adjusting the molecular structure.

Moreover, the biological and biomedical applications of the peptides are often well related to their nanostructuring through self-assembly.^{60,61} The current systems offer good candidates for evaluating the effects of the shape and size of nanostructures on their intended bioapplications. Our results show that the nanosheets exhibit the highest efficiency in encapsulating hydrophobic drug molecules, and that the nanosheets and nanorods produce better intracellular drug-delivery results than the nanofibers. These results thus offer a great promise for further exploiting the control of the self-assembled nanostructures as nanocarriers for drug loading and release.

■ ASSOCIATED CONTENT

Supporting Information

The Supporting Information is available free of charge on the ACS Publications website at DOI: [10.1021/acsmami.7b11681](https://doi.org/10.1021/acsmami.7b11681).

SANS data fitting, CD and FTIR characterization of the secondary structures, TEM morphologies of the peptide self-assembled structures at lower concentration and varied pH, XRD spectra of the peptide structures, fluorescence spectra of ANS with and without peptides, determination of the NR/DOX encapsulation efficiency as well as DOX release by fluorescence method, and cytotoxicity evaluation of different peptides ([PDF](#))

■ AUTHOR INFORMATION

Corresponding Authors

*E-mail: mwcao@upc.edu.cn (M.C.).

*E-mail: xuh@upc.edu.cn (H.X.).

*E-mail: j.lu@manchester.ac.uk (J.R.L.).

ORCID

Meiwen Cao: [0000-0002-3072-6780](https://orcid.org/0000-0002-3072-6780)

Jiqian Wang: [0000-0002-7525-5943](https://orcid.org/0000-0002-7525-5943)

Hai Xu: [0000-0002-5796-4404](https://orcid.org/0000-0002-5796-4404)

Jian R. Lu: [0000-0001-5648-3564](https://orcid.org/0000-0001-5648-3564)

Author Contributions

The manuscript was written through contributions of all of the authors. All of the authors have given approval to the final version of the manuscript.

Notes

The authors declare no competing financial interest.

■ ACKNOWLEDGMENTS

This work is supported by the National Natural Science Foundation of China (21473255, 21773310, and 11504431) and the Fundamental Research Funds for the Central

Universities (17CX02050). We thank the U.K. Engineering and Physical Science Research Council (EPSRC) under EP/F062966/1 and EPSRC and Innovate U.K. under KTP008143 and the ISIS Neutron and Muon Facility, STFC for award of neutron beam time to undertake the SANS work on LOQ.

■ REFERENCES

- (1) Liu, X.; Fei, J.; Wang, A.; Cui, W.; Zhu, P.; Li, J. Transformation of Dipeptide-Based Organogels into Chiral Crystals by Cryogenic Treatment. *Angew. Chem., Int. Ed.* **2017**, *56*, 2660–2663.
- (2) Fu, M.; Li, Q.; Sun, B.; Yang, Y.; Dai, L.; Nylander, T.; Li, J. Disassembly of Dipeptide Single Crystals Can Transform the Lipid Membrane into a Network. *ACS Nano* **2017**, *11*, 7349–7354.
- (3) Wang, J.; Liu, K.; Xing, R.; Yan, X. Peptide Self-Assembly: Thermodynamics and Kinetics. *Chem. Soc. Rev.* **2016**, *45*, 5589–5604.
- (4) Koley, P.; Gayen, A.; Drew, M. G. B.; Mukhopadhyay, C.; Pramanik, A. Design and Self-Assembly of a Leucine-Enkephalin Analogue in Different Nanostructures: Application of Nanovesicles. *Small* **2012**, *8*, 984–990.
- (5) Koley, P.; Pramanik, A. Nanostructures from Single Amino Acid-Based Molecules: Stability, Fibrillation, Encapsulation, and Fabrication of Silver Nanoparticles. *Adv. Funct. Mater.* **2011**, *21*, 4126–4136.
- (6) Arnon, Z. A.; Vitalis, A.; Levin, A.; Michaels, T. C. T.; Caflisch, A.; Knowles, T. P. J.; Adler-Abramovich, L.; Gazit, E. Dynamic Microfluidic Control of Supramolecular Peptide Self-Assembly. *Nat. Commun.* **2016**, *7*, No. 13190.
- (7) Abb, S.; Harnau, L.; Gutzler, R.; Rauschenbach, S.; Kern, K. Two-Dimensional Honeycomb Network through Sequence-Controlled Self-Assembly of Oligopeptides. *Nat. Commun.* **2016**, *7*, No. 10335.
- (8) Zhang, S. Fabrication of Novel Biomaterials through Molecular Self-Assembly. *Nat. Biotechnol.* **2003**, *21*, 1171–1178.
- (9) Zhao, X.; Pan, F.; Xu, H.; Yaseen, M.; Shan, H.; Hauser, C. A. E.; Zhang, S.; Lu, J. R. Molecular Self-Assembly and Applications of Designer Peptide Amphiphiles. *Chem. Soc. Rev.* **2010**, *39*, 3480–3498.
- (10) Löwik, D. W.; Leunissen, E. H.; van den Heuvel, M.; Hansen, M. B.; van Hest, J. C. Stimulus Responsive Peptide Based Materials. *Chem. Soc. Rev.* **2010**, *39*, 3394–3412.
- (11) Gazit, E. Self-Assembled Peptide Nanostructures: the Design of Molecular Building Blocks and Their Technological Utilization. *Chem. Soc. Rev.* **2007**, *36*, 1263–1269.
- (12) Rein, V. U. Peptide-Based Materials via Molecular Self-Assembly. In *Self-Assembled Peptide Nanostructures: Advances and Applications in Nanobiotechnology*; Jaime, C.-L., Luigi, S., Winnie, E. S., Eds.; CRC Press, Taylor & Francis Group: Boca Raton, 2012; pp 67–92.
- (13) Reches, M.; Gazit, E. Casting Metal Nanowires within Discrete Self-Assembled Peptide Nanotubes. *Science* **2003**, *300*, 625–627.
- (14) Xu, H.; Wang, Y.; Ge, X.; Han, S.; Wang, S.; Zhou, P.; Shan, H.; Zhao, X.; Lu, J. R. Twisted Nanotubes Formed from Ultrashort Amphiphilic Peptide I3K and Their Templating for the Fabrication of Silica Nanotubes. *Chem. Mater.* **2010**, *22*, 5165–5173.
- (15) Worthington, P.; Pochan, D. J.; Langhans, S. A. Peptide Hydrogels – Versatile Matrices for 3D Cell Culture in Cancer Medicine. *Front. Oncol.* **2015**, *5*, 92.
- (16) Dou, X.-Q.; Feng, C.-L. Amino Acids and Peptide-Based Supramolecular Hydrogels for Three-Dimensional Cell Culture. *Adv. Mater.* **2017**, No. 1604062.
- (17) Liu, K.; Yuan, C.; Zou, Q.; Xie, Z.; Yan, X. Self-Assembled Zinc/Cystine-Based Chloroplast Mimics Capable of Photoenzymatic Reactions for Sustainable Fuel Synthesis. *Angew. Chem., Int. Ed.* **2017**, *56*, 7876–7880.
- (18) Zou, Q.; Abbas, M.; Zhao, L.; Li, S.; Shen, G.; Yan, X. Biological Photothermal Nanodots Based on Self-Assembly of Peptide-Porphyrin Conjugates for Antitumor Therapy. *J. Am. Chem. Soc.* **2017**, *139*, 1921–1927.
- (19) Liu, K.; Xing, R.; Zou, Q.; Ma, G.; Möhwald, H.; Yan, X. Simple Peptide-Tuned Self-Assembly of Photosensitizers towards Anticancer Photodynamic Therapy. *Angew. Chem., Int. Ed.* **2016**, *55*, 3036–3039.

- (20) Yan, X.; He, Q.; Wang, K.; Duan, L.; Cui, Y.; Li, J. Transition of Cationic Dipeptide Nanotubes into Vesicles and Oligonucleotide Delivery. *Angew. Chem., Int. Ed.* **2007**, *46*, 2431–2434.
- (21) da Silva, E. R.; Walter, M. N.; Reza, M.; Castelletto, V.; Ruokolainen, J.; Connon, C. J.; Alves, W. A.; Hamley, I. W. Self-Assembled Arginine-Capped Peptide Bolaamphiphile Nanosheets for Cell Culture and Controlled Wettability Surfaces. *Biomacromolecules* **2015**, *16*, 3180–3190.
- (22) Dai, B.; Li, D.; Xi, W.; Luo, F.; Zhang, X.; Zou, M.; Cao, M.; Hu, J.; Wang, W.; Wei, G.; Zhang, Y.; Liu, C. Tunable assembly of amyloid-forming peptides into nanosheets as a retrovirus carrier. *Proc. Natl. Acad. Sci. U.S.A.* **2015**, *112*, 2996–3001.
- (23) Lim, Y.-b.; Lee, E.; Lee, M. Controlled Bioactive Nanostructures from Self-Assembly of Peptide Building Blocks. *Angew. Chem.* **2007**, *119*, 9169–9172.
- (24) Zhang, K.; Fang, H.; Chen, Z.; Taylor, J.-S. A.; Wooley, K. L. Shape Effects of Nanoparticles Conjugated with Cell-Penetrating Peptides (HIV Tat PTD) on CHO Cell Uptake. *Bioconjugate Chem.* **2008**, *19*, 1880–1887.
- (25) Geng, Y.; Dalheimer, P.; Cai, S.; Tsai, R.; Tewari, M.; Minko, T.; Discher, D. E. Shape Effects of Filaments Versus Spherical Particles in Flow and Drug Delivery. *Nat. Nanotechnol.* **2007**, *2*, 249–255.
- (26) Senguen, F. T.; Lee, N. R.; Gu, X.; Ryan, D. M.; Doran, T. M.; Anderson, E. A.; Nilsson, B. L. Probing Aromatic, Hydrophobic, and Steric Effects on the Self-Assembly of an Amyloid- β Fragment Peptide. *Mol. BioSyst.* **2011**, *7*, 486–496.
- (27) Stupp, S. I.; Zha, R. H.; Palmer, L. C.; Cui, H.; Bitton, R. Self-Assembly of Biomolecular Soft Matter. *Faraday Discuss.* **2013**, *166*, 9–30.
- (28) Woolfson, D. N.; Ryadnov, M. G. Peptide-Based Fibrous Biomaterials: Some Things Old, New and Borrowed. *Curr. Opin. Chem. Biol.* **2006**, *10*, 559–567.
- (29) Stupp, S. I. Self-Assembly and Biomaterials. *Nano Lett.* **2010**, *10*, 4783–4786.
- (30) Cui, H.; Webber, M. J.; Stupp, S. I. Self-Assembly of Peptide Amphiphiles: From Molecules to Nanostructures to Biomaterials. *Biopolymers* **2010**, *94*, 1–18.
- (31) Cui, H.; Muraoka, T.; Cheetham, A. G.; Stupp, S. I. Self-Assembly of Giant Peptide Nanobelts. *Nano Lett.* **2009**, *9*, 945–951.
- (32) Hamley, I. W.; Dehsorkhi, A.; Castelletto, V. Self-Assembled Arginine-Coated Peptide Nanosheets in Water. *Chem. Commun.* **2013**, *49*, 1850–1852.
- (33) Hamley, I. W.; Hutchinson, J.; Kirkham, S.; Castelletto, V.; Kaur, A.; Reza, M.; Ruokolainen, J. Nanosheet Formation by an Anionic Surfactant-like Peptide and Modulation of Self-Assembly through Ionic Complexation. *Langmuir* **2016**, *32*, 10387–10393.
- (34) Xu, H.; Wang, J.; Han, S.; Wang, J.; Yu, D.; Zhang, H.; Xia, D.; Zhao, X.; Waigh, T. A.; Lu, J. R. Hydrophobic-Region-Induced Transitions in Self-Assembled Peptide Nanostructures. *Langmuir* **2009**, *25*, 4115–4123.
- (35) Hamley, I. W. The Amyloid Beta Peptide: A Chemist's Perspective. Role in Alzheimer's and Fibrillization. *Chem. Rev.* **2012**, *112*, 5147–5192.
- (36) Castelletto, V.; Nutt, D. R.; Hamley, I. W.; Buck, S.; Cenker, C.; Olsson, U. Structure of single-wall peptide nanotubes: in situ flow aligning X-ray diffraction. *Chem. Commun.* **2010**, *46*, 6270–6272.
- (37) Sawaya, M. R.; Sambashivan, S.; Nelson, R.; Ivanova, M. I.; Sievers, S. A.; Apostol, M. I.; Thompson, M. J.; Balbirnie, M.; Wiltzius, J. J.; McFarlane, H. T.; Madsen, A. O.; Riek, C.; Eisenberg, D. Atomic Structures of Amyloid Cross- β Spines Reveal Varied Steric Zippers. *Nature* **2007**, *447*, 453–457.
- (38) Nelson, R.; Sawaya, M. R.; Balbirnie, M.; Madsen, A. O.; Riek, C.; Grothe, R.; Eisenberg, D. Structure of the Cross- β Spine of Amyloid-Like Fibrils. *Nature* **2005**, *435*, 773–778.
- (39) Han, S.; Cao, S.; Wang, Y.; Wang, J.; Xia, D.; Xu, H.; Zhao, X.; Lu, J. R. Self-Assembly of Short Peptide Amphiphiles: The Cooperative Effect of Hydrophobic Interaction and Hydrogen Bonding. *Chem. – Eur. J.* **2011**, *17*, 13095–13102.
- (40) Erdogan, H.; Babur, E.; Yilmaz, M.; Candas, E.; Gordesel, M.; Dede, Y.; Oren, E. E.; Demirel, G. B.; Ozturk, M. K.; Yavuz, M. S.; Demirel, G. Morphological Versatility in the Self-Assembly of Val-Ala and Ala-Val Dipeptides. *Langmuir* **2015**, *31*, 7337–7345.
- (41) Moudrakovski, I.; Soldatov, D. V.; Ripmeester, J. A.; Sears, D. N.; Jameson, C. J. Xe NMR Lineshapes in Channels of Peptide Molecular Crystals. *Proc. Natl. Acad. Sci. U.S.A.* **2004**, *101*, 17924–17929.
- (42) Kyte, J.; Doolittle, R. F. A Simple Method for Displaying the Hydropathic Character of a Protein. *J. Mol. Biol.* **1982**, *157*, 105–132.
- (43) Castelletto, V.; Hamley, I. W. Self Assembly of a Model Amphiphilic Phenylalanine Peptide/Polyethylene Glycol Block Copolymer in Aqueous Solution. *Biophys. Chem.* **2009**, *141*, 169–174.
- (44) Shao, H.; Parquette, J. R. Controllable Peptide-Dendron Self-Assembly: Interconversion of Nanotubes and Fibrillar Nanostructures. *Angew. Chem., Int. Ed.* **2009**, *48*, 2525–2528.
- (45) Zhao, Y.; Wang, J.; Deng, L.; Zhou, P.; Wang, S.; Wang, Y.; Xu, H.; Lu, J. R. Tuning the Self-Assembly of Short Peptides via Sequence Variations. *Langmuir* **2013**, *29*, 13457–13464.
- (46) Zhao, Y.; Deng, L.; Wang, J.; Xu, H.; Lu, J. R. Solvent Controlled Structural Transition of KI4K Self-Assemblies: from Nanotubes to Nanofibrils. *Langmuir* **2015**, *31*, 12975–12983.
- (47) Ziserman, L.; Lee, H. Y.; Raghavan, S. R.; Mor, A.; Danino, D. Unraveling the Mechanism of Nanotube Formation by Chiral Self-Assembly of Amphiphiles. *J. Am. Chem. Soc.* **2011**, *133*, 2511–2517.
- (48) Juban, M. M.; Javadpour, M. M.; Barkley, M. D. Circular Dichroism Studies of Secondary Structure of Peptides. In *Methods in Molecular Biology*; Shafer, W. M., Ed.; Humana Press Inc.: Totowa, NJ, 1997; Chapter Antibacterial Peptide Protocols.
- (49) Lee, N. R.; Bowerman, C. J.; Nilsson, B. L. Effects of Varied Sequence Pattern on the Self-Assembly of Amphipathic Peptides. *Biomacromolecules* **2013**, *14*, 3267–3277.
- (50) Haris, P. I.; Chapman, D. The Conformational Analysis of Peptides Using Fourier Transform IR Spectroscopy. *Biopolymers* **1995**, *37*, 251–263.
- (51) Pelton, J. T.; McLean, L. R. Spectroscopic Methods for Analysis of Protein Secondary Structure. *Anal. Biochem.* **2000**, *277*, 167–176.
- (52) Blake, C.; Serpell, L. Synchrotron X-ray Studies Suggest That the Core of the Transthyretin Amyloid Fibril Is a Continuous β -sheet Helix. *Structure* **1996**, *4*, 989–998.
- (53) Sunde, M.; Serpell, L. C.; Bartlam, M.; Fraser, P. E.; Pepys, M. B.; Blake, C. C. F. Common Core Structure of Amyloid Fibrils by Synchrotron X-ray Diffraction. *J. Mol. Biol.* **1997**, *273*, 729–739.
- (54) Serpell, L. C. Alzheimer's Amyloid Fibrils: Structure and Assembly. *Biochim. Biophys. Acta, Mol. Basis Dis.* **2000**, *1502*, 16–30.
- (55) Wu, C.; Wang, Z.; Lei, H.; Duan, Y.; Bowers, M. T.; Shea, J. E. The Binding of Thioflavin T and Its Neutral Analog BTA-1 to Protofibrils of the Alzheimer's Disease $\text{A}\beta(16-22)$ Peptide Probed by Molecular Dynamics Simulations. *J. Mol. Biol.* **2008**, *384*, 718–729.
- (56) Carter, D. B.; Chou, K. C. A Model for Structure-Dependent Binding of Congo Red to Alzheimer β -Amyloid Fibrils. *Neurobiol. Aging* **1998**, *19*, 37–40.
- (57) Mao, X.; Guo, Y.; Wang, C.; Zhang, M.; Ma, X.; Liu, L.; Niu, L.; Zeng, Q.; Yang, Y.; Wang, C. Binding Modes of Thioflavin T Molecules to Prion Peptide Assemblies Identified by Using Scanning Tunneling Microscopy. *ACS Chem. Neurosci.* **2011**, *2*, 281–287.
- (58) Marchesan, S.; Qu, Y.; Waddington, L. J.; Easton, C. D.; Glattauer, V.; Lithgow, T. J.; McLean, K. M.; Forsythe, J. S.; Hartley, P. G. Self-Assembly of Ciprofloxacin and a Tripeptide into an Antimicrobial Nanostructured Hydrogel. *Biomaterials* **2013**, *34*, 3678–3687.
- (59) Hayashida, O.; Ono, K.; Hisaeda, Y.; Murakami, Y. Specific Molecular Recognition by Chiral Cage-Type Cyclophanes Having Leucine, Valine, and Alanine Residue. *Tetrahedron* **1995**, *51*, 8423–8436.
- (60) McGuinness, K.; Khan, I. J.; Nanda, V. Morphological Diversity and Polymorphism of Self-Assembling Collagen Peptides Controlled by Length of Hydrophobic Domains. *ACS Nano* **2014**, *8*, 12514–12523.

- (61) Castillo, J.; Andersen, K. B.; Svendsen, W. E.; Castillo, J.; Andersen, K. B.; Svendsen, W. E. Self-Assembled Peptide Nanostructures for Biomedical Applications: Advantages and Challenges. In *Biomaterials Science and Engineering*; Pignatello, R., Pignatello, R., Eds.; InTech, 2011.